JOURNAL OF MATERIALS SCIENCE **40** (2005) 3347–3353

Characterization of low angle grain boundaries in yttrium orthovanadate

JOEL B. LEBRET, M. GRANT NORTON*, DAVID F. BAHR, DAVID P. FIELD, KELVIN G. LYNN
School of Mechanical and Materials Engineering, Washington State University, Pullman, WA 99164, USA
E-mail: norton@mme.wsu.edu

Single crystals of Nd:YVO_4 grown with the Czochralski technique frequently exhibit light scattering defects that are detrimental to their lasing and optical properties. Defects in the form of low angle grain boundaries have been characterized in what are nominally 'single crystals'. The misorientation angles of the boundaries were determined to be typically $<1^\circ$, which corresponds to formation energies of approximately 1 Jm^{-2}. It was found that dislocations generated during crystal growth and cooling have enough mobility in certain growth directions to form low angle grain boundaries through polygonization. Despite the relatively high energies the boundaries were stable, being immobile at annealing temperatures up to 97% of the melting point (2083 K). Suggestions are made to reduce or eliminate polygonization, including the addition of atoms with a size either much larger or smaller than Y^{3+}.

1. Introduction

Neodymium doped yttrium orthovanadate (Nd:YVO_4) has been shown to have desirable properties as a solid state laser host material and is one of the most efficient hosts for diode laser pumped applications. It has a large absorption coefficient, broad absorption bandwidth, large stimulated emission cross-section, and low lasing threshold [1–4]. The main obstacle for proliferation of Nd:YVO_4 is the challenge of growing large, defect-free single crystals.

YVO_4 is tetragonal ($a = 0.71192$ nm, $c = 0.62898$ nm) and of zircon type symmetry (point group $I4_1/amd$). YVO_4 is a positive uniaxial crystal and is highly birefringent; these properties, combined with its wide transparency range, make it ideal for optical applications such as fibre optic isolators and beam displacers, circulators, and polarizers. YVO_4 has better temperature stability, physical and mechanical properties than calcite ($CaCO_3$), easier handling and workability than rutile (TiO_2), and higher birefringence than $LiNbO_3$. Zhang *et al.* have recently shown that a YVO_4 bicrystal device can be used to achieve amphoteric refraction as well as zero reflection loss [5]. The ability to steer light without reflection is important in realizing extremely efficient high power optics.

Several techniques have been explored for the growth of single crystal Nd:YVO_4. Crystals of large diameter and good quality have been grown with the Czochralski (Cz) technique [6]; other successful growth methods include float zone (FZ) [7], laser heated pedestal growth [8], flux growth [9], and top-seeded solution growth [10]. The Cz technique has been selected as the best growth method since it is capable of producing crystals of large diameter, although some problems with crystal quality still need to be addressed.

Light scattering defects such as voids or inclusions [11], residual stress from processing, colour centres, stoichiometric fluctuations [10, 12, 13], and low angle grain boundaries (GBs) [14] have all been observed in Nd:YVO_4 crystals and are problematic for maintaining high laser efficiency. Through appropriate selection of constituent materials and optimizing the growth parameters such as atmosphere, pull rates and temperatures, some of these problems can be reduced or avoided. Low angle GBs remain an elusive defect, as there has yet to be a means of eliminating them in the growth process of large crystals.

Low angle GBs in Nd:YVO_4 have been identified using polarized light microscopy [14]. It has been suggested that they form due to migration of dislocations introduced during crystal growth and cooling. Low angle GBs nearly parallel to the *a*-face have been noted in crystals grown along [100] or [010] (henceforth labelled as *a*-grown). Similar boundaries are not observed in crystals grown along [001] (*c*-grown); it has also been found that *c*-grown crystals have a much higher tendency to crack. In this present paper, low angle GBs in Nd:YVO_4 have been characterized and possible formation mechanisms examined with the intent that a better understanding might lead to improved growth parameters and overall crystal quality.

* Author to whom all correspondence should be addressed.

2. Experimental techniques

Boules of Nd:YVO_4 grown with the Cz method in the *a*- and *c*-directions were secured from commercial vendors for defect characterization. The boules were typically ∼3 cm in diameter. The crystals had nominal Nd concentrations varying from 0.27–2.0% where the percentage of Nd is given as a substitutional amount for Y. Nd is introduced by the addition of Nd_2O_3 and the appropriate excess of V_2O_5 to maintain crystal stoichiometry. The crystals were grown above 2083 K in an Ir crucible with pull rates ranging from 0.5–3 mmh^{-1} and rotation rates from 10–30 rpm. The crystals were grown under a small (∼2%) O_2 atmosphere to avoid oxygen vacancies, which result in non-stoichiometric light-scattering phases. The crystals had been inspected visually by the vendors and qualitatively rated for defects. Low angle GBs produce slight changes in the refractive properties that can be detected with a keen eye.

Polarized light microscopy was used to better understand the extent of the non-uniformity of the crystals. The samples analyzed included Cz grown boules, boule caps (the region of the boule just below the seed crystal), and finished laser elements. Where necessary, samples were cut with a diamond embedded saw, ground from 320 to 1200 grit SiC and polished through 0.05 μm diamond paste with gold-label cloth and oil suspension. The samples were analyzed using a Nikon Optiphot-Pol transmitted light polarized microscope near a position of extinction. Images were captured with a SPOT CCD camera and software.

Samples were further analyzed with scanning electron microscopy (SEM) for topographical and crystallographic information. Samples were prepared for electron backscattered diffraction (EBSD) analysis using the metallographic techniques described above. Some samples were coated with an amorphous carbon layer to reduce charging. EBSD was used to determine the approximate boundary misorientation. A scan area of 780 by 2104 μm was used with a step size of 15 μm. The samples were analyzed with a CamScan Series 4 SEM operated at 20 keV and equipped with a DigiView II slow scan CCD camera and TSL data collection and analysis software.

Samples prepared for topographical analysis of etch pits were polished and subsequently etched in HNO_3 at about 373 K for times ranging from 40 min to 2 h. The samples were heated and allowed to cool, at a rate of $\sim 4^\circ\ min^{-1}$, in the solution to avoid thermal shock. The etch pits were imaged with a JEOL JSM-6400 SEM operated at 20 keV.

TEM specimens were prepared from crystals that contained low angle GBs. Standard specimen preparation techniques were used with final perforation achieved using a 3:1 solution of H_3PO_4 and H_2SO_4 at 393 K. Perforation typically occurred within 10–15 min. A final cleaning was performed in an ion mill with 4.5 kV Ar^+ for 1 h. Some samples were carbon coated to reduce charging. The samples were analyzed with a Phillips CM 200 TEM operated at 200 keV.

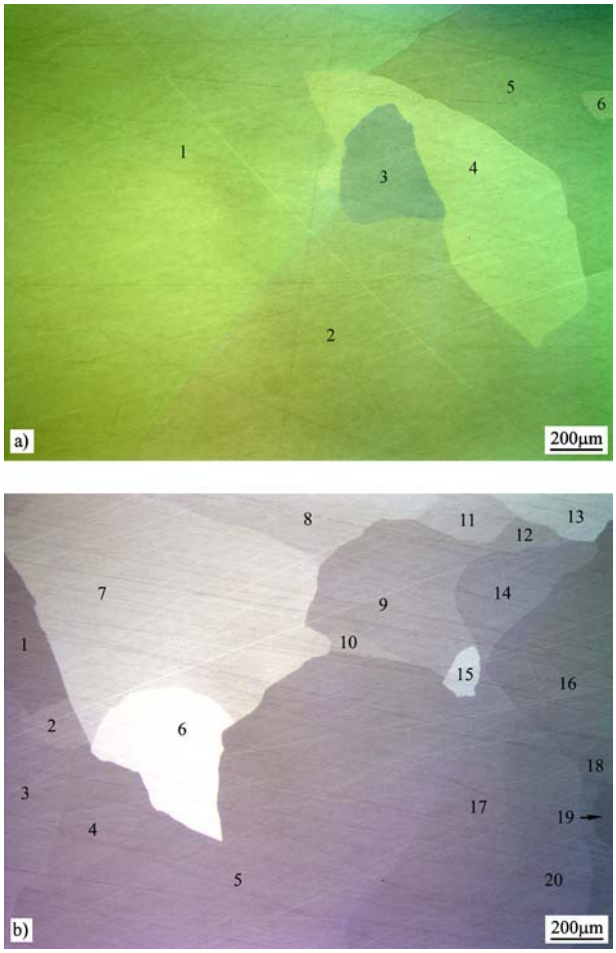

Figure 1 Polarized light microscope image of low angle GBs from (a) the boule cap, and (b) bottom face. Note that crystallite 3 from (a) is the same as 6 from (b); the misorientation of the boundaries increased as the crystal grew.

3. Results

Fig. 1 shows an example of distinct crystallites, separated by low angle GBs, on the growth face of an *a*-grown Nd:YVO_4 boule. From inspection of the top and bottom faces of the boule it was apparent that these features increase in number and misorientation as the crystal grows. Crystallites of greater misorientation result in higher contrast when viewed with polarized light. It was possible to track the location and shape of the crystallites through the entire length of the crystal. Boule caps were examined to determine where in the growth process the low angle GBs form. Crystallites were identified at the topmost and centre part of the boule cap (Fig. 1a). Boundaries formed early in the growth process and lead to many subsequent boundaries throughout the crystal, as can be seen in Fig. 1b, which was taken from the bottom face of the boule, 39 mm from the cap.

Crystals that had low ratings for the number of light scattering boundaries from the vendor's initial visual inspection were found to contain numerous boundaries when inspected with polarized light. In fact, the number of low angle GBs for the low rated crystals was very close to the number in high rated crystals as illustrated in Fig. 2. As expected, contrast variation was greater in images in which the boundaries could be seen readily by

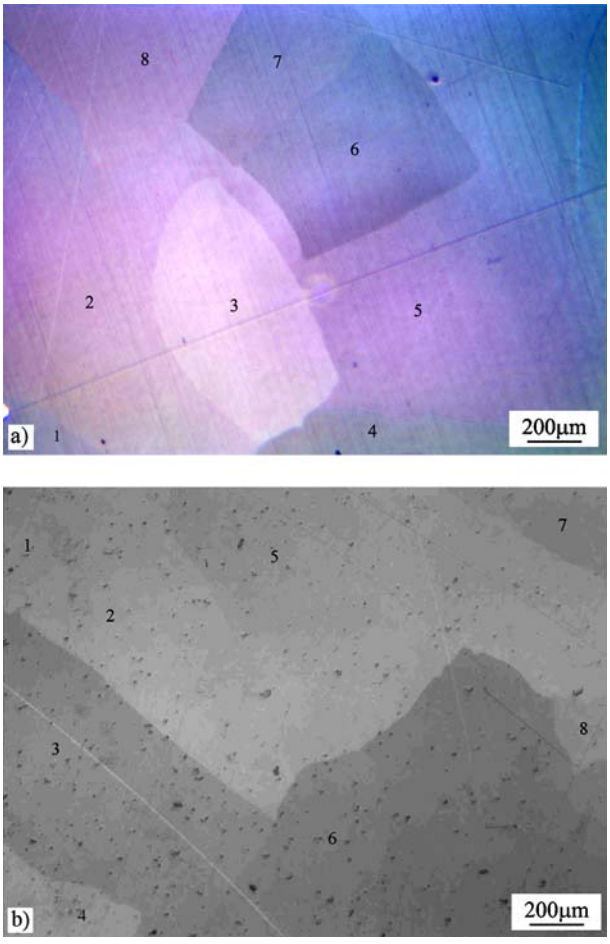

Figure 2 Polarized light microscope image of crystallites in samples that were inspected visually and rated from 1–5 (1 = best, 5 = worst): (a) 1, (b) 5.

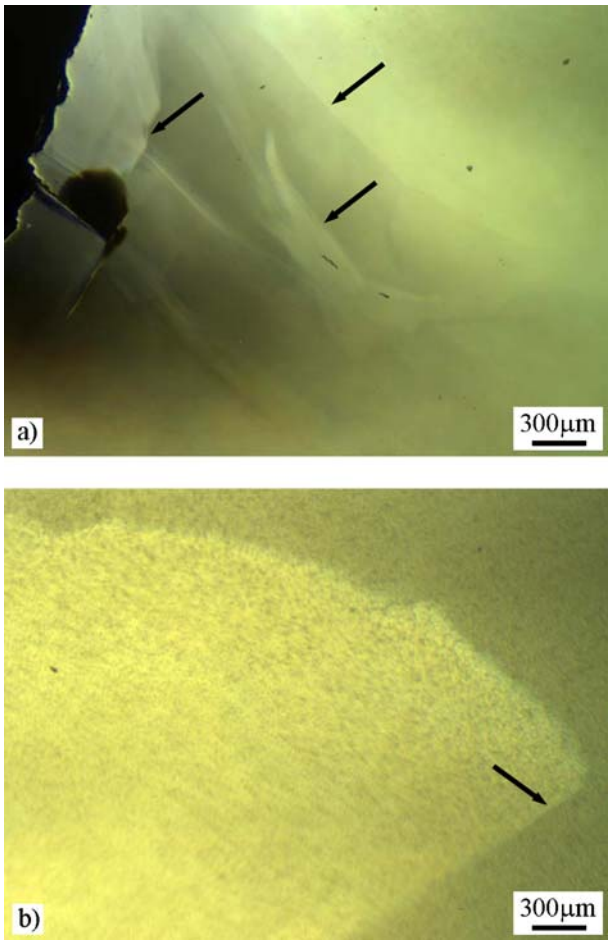

Figure 3 Polarized light microscope image of microcracks in *c*-grown boules were visible (a) under and (b) at the surface of the crystals. The arrows denote the microcrack regions.

visual inspection because of the larger misorientation between crystallites in these samples.

Crystals grown in the *c*-direction do not exhibit polarized light contrast since the crystals are optically isotropic when viewed along [001]. Features with similar appearance to low angle GBs were noted on *c*-grown crystals, but these were actually microcracks. Two examples of microcracking are shown in Figs 3a and b. It was noted that on all the *c*-grown samples that contained light-scattering defects there were large cracks in the same region.

It was found that Nd:YVO_4 etches preferentially along the *a*-directions. Etch pits on the *a*-faces were found to be at low angle GBs and artefacts on the surface such as scratches (Fig. 4). In the *c*-grown crystals, the distribution of etch pits were much more uniform as shown in Fig. 5a. Etch pits on the *c*-faces were observed to be square, unlike those on the *a*-faces. Numerous microcracks were noted (Fig. 5b) on *c*-grown samples, which corresponded with the features exhibiting a change in refractive properties from Fig. 3.

EBSD was performed on several samples known to contain low angle GBs to determine the approximate misorientation. A directional map of the crystal along the radial direction revealed a misorientation measured to be about $1.4^\circ \pm 1^\circ$ (Fig. 6). The misorientation of the crystallite was found to vary along the boundary length. It is possible that additional boundaries adjoining the cell may exist which could not be resolved with EBSD. Since the accepted sensitivity of EBSD to misorientation is $>0.5^\circ$, determination of the exact misorientation of the low angle GB is not possible with this method.

Fig. 7 shows a bright field TEM image of a periodic array of dislocations that form a low angle GB. The length of the boundary that was captured in the electron transparent area of the sample extended for 35 μm. In another region a boundary extending for more than 40 μm was found. The average dislocation spacing was measured to be 250 and 50 nm, respectively. On-axis Kikuchi patterns taken from either side of the boundary shown in Fig. 7 were compared and the misorientation angle of the boundary was determined to be 0.14° by calculating direction cosines formed by the pattern centre and two common points on each pattern.

4. Discussion

Since comparable numbers of low angle GBs were observed with polarized light on Nd:YVO_4 crystals with low and high rating, the visual inspection technique is not adequate for accurate description of the number of boundaries present. However, contrast differences were noted and could be an indication of the extent of boundary misorientation.

The etch pit density and distribution is important in understanding the mechanisms of low angle GB

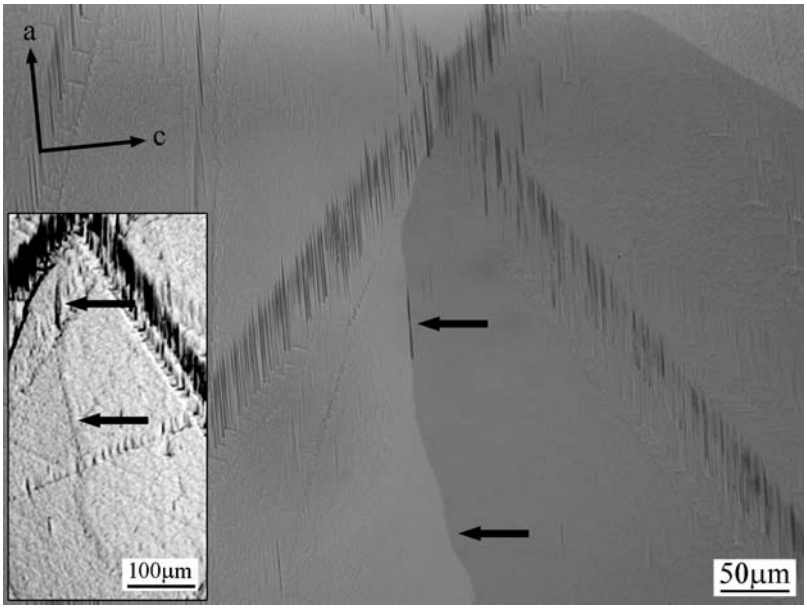

Figure 4 Polarized light microscope image of rectangular dislocation etch pits located at a low angle GB in an *a*-grown crystal; the inset, a reflected light image shows etch pits at the same boundary seen with polarized light. The arrows denote similar regions in both images.

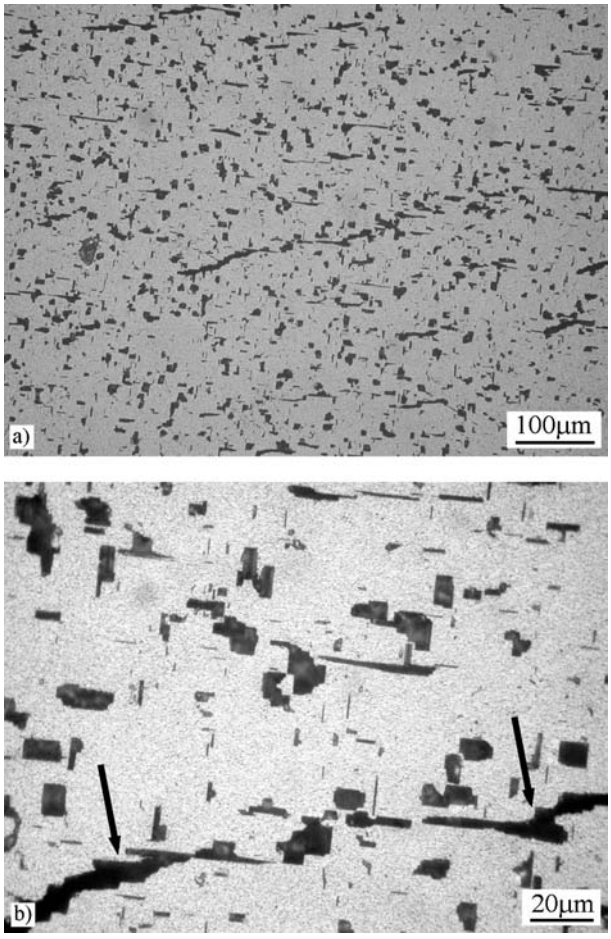

Figure 5 Reflected light images showing (a) an even distribution of etch pits, and (b) etched microcracks in *c*-grown crystals (denoted with arrows).

formation. The presence of dislocations has been verified in both *a*- and *c*-grown crystals. The dislocations in *a*-grown crystals tend to be localized on low angle GBs whereas the dislocations in *c*-grown crystals are evenly distributed. This observation implies increased dislocation mobility and/or stress along certain directions.

Using the dislocation spacing D and the Burgers vector b, the misorientation angle can be determined. For unit translation dislocations of the type $\frac{1}{2}[111]$ the magnitude of the Burgers vector is 0.594 nm [15]. With an average dislocation spacing shown in Fig. 7 of 250 nm, the misorientation angle θ was calculated to be about 0.14°. This is in excellent agreement with the calculations made from the Kikuchi patterns of the same boundary.

With a known misorientation angle it is possible to calculate the energy required to form the GB. Using the Read and Shockley formula derived for a boundary composed of an array of dislocations, the energy E can be found by [16]:

$$E = E_0\theta[A - \ln\theta] \tag{1}$$

where A is an integration constant ranging from about 0.345 to 0.5, and E_0 is the elastic strain energy for an edge dislocation, which can be found using Equation 2.

$$E_0 = \frac{Gb}{4\pi(1-\nu)} \tag{2}$$

For Nd:YVO_4, the shear modulus G is 50 GPa and Poisson's ratio ν is 0.33 [17], which gives $E_0 = 3.53\ \mathrm{Jm}^{-2}$. With a misorientation of 0.14° and taking a value of 0.4 for A, an energy of $1.17\ \mathrm{Jm}^{-2}$ is obtained. For a boundary with similar misorientation in Cu an energy of $0.46\ \mathrm{Jm}^{-2}$ is obtained [18]. The energy of these low angle GBs in Nd:YVO_4 is thus quite large when compared to fcc metals, a consequence of the large shear modulus and Burgers vector, but the boundaries appeared very stable. Examination of low angle GBs in finished laser elements revealed no change in the boundary locations and shapes or sizes of the crystallites after annealing at 1973 K and then 2023 K for five

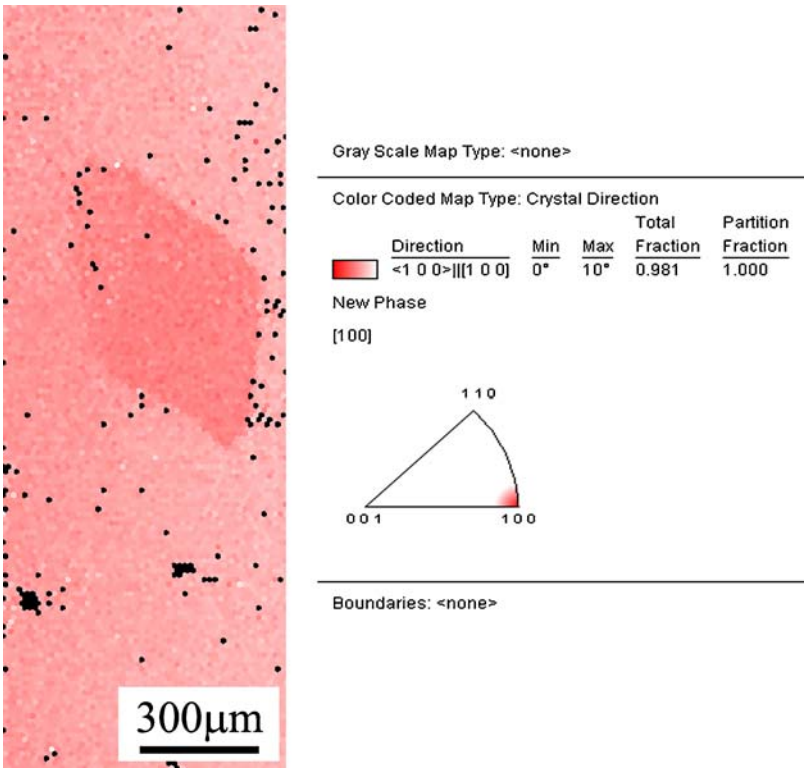

Figure 6 EBSD image showing a crystallite with a misorientation determined to be 1.4° ± 1°.

hours each. The melting temperature of YVO_4 is 2083 K and thus it is not feasible to remove these boundaries through annealing.

Low angle GBs are not unique to Nd:YVO_4; other single crystals such as rutile (TiO_2), $LiNbO_3$, $LiTaO_3$, $YAlO_3$, Al_2O_3, and $GdVO_4$ also exhibit this defect from growth. Of particular interest are Nd:$GdVO_4$, rutile, and yttrium orthoaluminate perovskite, $YAlO_3$, (YAP) as they have properties very comparable to Nd:YVO_4 and are used in similar applications. Examination of low angle GB formation in these materials may provide insight into how similar boundaries form in Nd:YVO_4.

Dislocations are introduced during growth due to thermal stresses and defects in the crystal or seed material. Other factors that increase dislocation density are inclusions, crystal diameter, and growth rate [19, 20]. Defects in the seed crystal are another source of dislocations and low angle GB formation. Any remaining crystallites floating on the surface of the melt may act as nucleation sites and it is important to superheat the material 50–100°C above the melting temperature for at least one hour [19]. Thermal stresses due to anisotropy in thermal expansion coefficients have been shown to be a major source of stress during cooling [21, 22]. Differential cooling between the crystal centre and surface coupled with anisotropic contraction produces a radial hoop stress in the material that can activate slip systems at high temperatures, allowing dislocation glide. The stress depends on the Burgers vector of the dislocation, the growth plane, and thermal expansion coefficients [23]. Movement of these dislocations at high temperatures is capable of resulting in polygonization as dislocations move into lower energy configurations. Polygonization is known to be responsible for low angle GB formation in YAP [22] and rutile [24, 25]. It is proposed that polygonization occurs in YVO_4.

The shear stress required to move a dislocation in a crystal at room temperature can be estimated using:

$$\tau_p \approx \frac{2G}{1-\nu} e^{-[2\pi a/(1-\nu)b]} \tag{3}$$

where a is the distance between slip planes and b is the distance between atoms in the slip direction, typically the ratio a/b is taken to be unity. Using the published values for G and ν, τ_p is 12.6 MPa.

The critical resolved shear stress for dislocation movement on the $(1\bar{1}2)[\bar{1}11]$ system was calculated for stresses on [100] and [001]. The angle ϕ, between the slip plane normal and the stress directions, and the angle λ, between the slip direction and the stress directions were calculated and the critical resolved shear stress, τ_R then determined. It was calculated that $\tau_{[100]} = 0.207\,\sigma$ and $\tau_{[001]} = 0.530\,\sigma$. With the value for τ_p used as the critical shear stress, the applied stress, σ, can be calculated to be 61.0 MPa for $\sigma_{[100]}$ and 23.8 MPa for $\sigma_{[001]}$. Since the thermal expansion coefficients are known it is possible to calculate the change in temperature for which the required stresses will be produced using

$$\sigma = E\alpha\Delta T \tag{4}$$

For Nd:YVO_4, $E = 133$ GPa, $\alpha_a = 2.2 \times 10^{-6}$ K^{-1}, and $\alpha_c = 8.4 \times 10^{-6}$ K^{-1} [26], so ΔT required to produce sufficient stress for dislocation movement is 21.3°C for stress along [001] and 208.5°C along [100] and [010]. This stress, combined with the stress from lattice mismatch (due to Nd concentration and segregation) and with the increased ductility at high

Figure 7 Bright field TEM image of a periodic array of dislocations forming a low angle GB.

temperatures (due to thermal activation), is enough to overcome the energy barrier and cause slip along [001] for relatively small changes in temperature. Based on these calculations, it is apparent how the orientation of crystal growth impacts the resulting dislocation mobility and thus the propensity to form low angle GBs. This approach explains why low angle GBs are not observed in *c*-grown crystals. Isotropic contraction along [100] and [010], combined with smaller stresses, is not enough to overcome the energy required to move the dislocations into lower energy configurations. Since dislocations perpendicular to [001] are locked, they are not able to relieve stress through low angle GB formation; consequently, *c*-grown crystals tend to crack.

If the movement of dislocations were hindered, it might be possible to stop the polygonization process in *a*-grown crystals. One such way to pin dislocations would be through solid solution strengthening. The stresses effectively prohibit dislocation motion when they encounter the lattice near the solute ion. Solid solution strengthening has been shown to be an effective method to reduce low angle GBs in rutile [25, 27–29]. Rutile is grown with Cz, FZ, and Verneuil growth techniques and like Nd:YVO_4, it exhibits low angle GBs that cause scattering of light. It has been shown for rutile that controlling O_2 atmosphere reduces the number of low angle GBs but the formation of opaque oxygen vacancies can be problematic. Alternately, it has been shown that addition of approximately 0.4 at% ZrO_2, Sc_2O_3, and Al_2O_3 were effective in eliminating low angle GBs due to dislocation pinning. The ionic radius of Al^{3+} is 0.051 nm, Zr^{4+} is 0.079 nm and Sc^{3+} is 0.081 nm, compared to Ti^{4+}, which is 0.068 nm. Of the various additions, Al_2O_3 appeared to be the most effective in suppressing the formation of low angle GBs.

The ionic radii of Nd^{3+} and Y^{3+} are 0.108 and 0.093 nm, respectively. It has been observed in industry and with preliminary observations in our group that crystals with significantly lower Nd concentrations (for e.g., 0.27% compared to 2.0%) exhibit a higher number of low angle GBs, thus it is probable that the Nd^{3+} ions contribute somewhat to dislocation pinning; a greater difference in ionic radii may contribute to a further extent. It is suggested that the addition of a small amount of Al^{3+}, might be an effective way to eliminate low angle GBs in Nd:YVO_4. However, since dislocation movement producing these boundaries reduces stress in the crystal, problems might be encountered with crystal fracture as seen with *c*-grown Nd:YVO_4.

5. Conclusions

Etching of *a*-grown Nd:YVO_4 crystals has revealed that dislocations are primarily located at low angle Gbs. The boundary misorientations were shown to vary from $\sim 0.1^\circ$ to $\sim 1^\circ$.

The anisotropic thermal expansion coefficient in Nd:YVO_4 produces a larger stress along [001] in *a*-grown crystals. At high temperatures, thermal stresses from anisotropic compression during cooling provide adequate stress for dislocation motion. It is energetically favourable for dislocations to form low angle GBs; the formation energy of the boundaries analyzed is between 1–2 Jm^{-2}. Low angle Gbs are not as likely to form in *c*-grown crystals due to the higher stresses required for dislocation motion; in this orientation, these stresses are not provided because of the isotropic compression during cooling. Crystals grown in the *c*-direction thus have a higher degree of internal stress and typically exhibit microcracking.

If the movement of dislocations were hindered, it might be possible to stop the polygonization process in YVO_4. It appears that Nd^{3+} ions contribute somewhat to dislocation pinning, but a greater difference in radius might contribute to a larger extent.

Acknowledgements

The authors thank Scotty Cornelius for his assistance with polarized light microscopy. This work was

performed with financial assistance from the Department of Defence, Joint Electromagnetics Technology Program Office, under the Assistant Secretary of Defense for Command, Control, Communications and Intelligence (ASD/C^3I), under Contract No. N66001-00-*C*-6008, through a subcontract from VLOC Incorporated, a subsidiary of II-VI Incorporated.

References

1. J. R. O'CONNOR, *Appl. Phys. Lett.* **9** (1966) 407.
2. P. P. YANEY and L. G. DE SHAZER, *J. Opt. Soc. Am.* **66** (1976) 1405.
3. A. W. TUCKER, M. BIRNBAUM, C. L. FINCHER and L. G. DE SHAZER, *J. Appl. Phys.* **47** (1976) 232.
4. R. A. FIELDS, M. BIRNBAUM and C. L. FINCHER, *Appl. Phys. Lett.* **51** (1987) 1885.
5. Y. ZHANG, B. FLUEGAL and A. MASCARENHAS, *Phys. Rev. Lett.* **91** (2003) 157404.
6. H. M. DESS and S. R. BOLIN, *Trans. TMS-AIME* **239** (1967) 359.
7. T. SHONAI, M. HIGUCHI and K. KODAIRA, *Mater. Res. Bull.* **35** (2000) 225.
8. C. GOUTAUDIER, F. S. ERMENEUX, M. T. COHEN-ADAD, R. MONCORGE, M. BETTINELLI, and E. CAVALLI, *ibid.* **33** (1998) 1457.
9. T. KATSUMATA, H. TAKASHIMA, H. OZAWA, K. MATSUURA and Y. NOBE, *J. Cryst. Growth* **148** (1995) 193.
10. S. ERDEI, B. M. JIN, F. W. AINGER, B. KESZEI, J. VANDLIK and A. SUVEGES, *ibid.* **172** (1997) 466.
11. R. C. ROPP, *Mat. Res. Bull.* **10** (1975) 271.
12. T. KATSUMATA, H. TAKASHIMA, T. MICHINO and Y. NOBE, *Mat. Res. Bull.* **29** (1994) 1247.
13. L. SANGALETTI, B. ALLIERI, L. E. DEPERO, M. BETTINELLI, K. LEBBOU and R. MONCORGE, *J. Cryst. Growth* **198/199** (1999) 454.
14. B. Q. HU, Y. Z. ZHANG, X. WU and X. L. CHEN, *ibid.* **226** (2001) 511.
15. D. E. EAKINS, J. B. LEBRET, M. G. NORTON and D. F. BAHR, *ibid.* **266** (2004) 411.
16. W.T. READ, in "Dislocations in Crystals" (McGraw-Hill, New York, 1953) p. 155.
17. X. PENG, A. ASUNDI, Y. CHEN and Z. XIONG, *Appl. Opt.* **40** (2001) 1396.
18. H. G. VAN BUEREN, in "Imperfections in Crystals" (North Holland Publishing Company, Amsterdam, 1961) p. 443.
19. L. QIN, X. MENG, J. ZHANG, L. ZHU, H. ZHANG, B. XU and H. JIANG, *J. Cryst. Growth* **242** (2002) 183.
20. T. SHONAI, M. HIGUCHI, K. KODAIRA, T. OGAWA, S. WADA and H. MACHIDA, *J. Cryst. Growth* **241** (2002) 159.
21. B. COCKAYNE, B. LENT, J. S. ABELL and I. R. HARRIS, *J. Mater. Sci.* **8** (1973) 871.
22. B. COCKAYNE, B. LENT, J. S. ABELL and P. M. MARQUIS, *J. Mater. Sci.* **10** (1975) 1874.
23. H. KLAPPER and H. KUPPERS, *Acta Cryst. A* **29** (1973) 495.
24. M. G. BLANCHIN and G. FONTAINE, *Phys. Stat. Sol. A* **29** (1975) 491.
25. M. HIGUCHI, T. HOSOKAWA and S. KIMURA, *J. Cryst. Growth* **112** (1991) 354.
26. H. J. ZHANG, L. ZHU, X. L. MENG, Z. H. YANG, C. Q. WANG, W. T. YU, Y. T. CHOW and M. K. LU, *Cryst. Res. Technol.* **34** (1999) 1011.
27. M. HIGUCHI, K. HATTA, J. TAKAHASHI, K. KODAIRA, H. KANEDA and J. SAITO, *J. Cryst. Growth* **208** (2000) 501.
28. M. HIGUCHI and K. KODAIRA, *ibid.* **123** (1992) 495.
29. M. HIGUCHI, J. TAKAHASHI and K. KODAIRA, *ibid.* **125** (1992) 125.

Received 15 December 2004
and accepted 1 February 2005